REVIEW

Perfusion-driven Intravoxel Incoherent Motion (IVIM) MRI in Oncology: Applications, Challenges, and Future Trends

Mami Iima[1,2*]

Recent developments in MR hardware and software have allowed a surge of interest in intravoxel incoherent motion (IVIM) MRI in oncology. Beyond diffusion-weighted imaging (and the standard apparent diffusion coefficient mapping most commonly used clinically), IVIM provides information on tissue microcirculation without the need for contrast agents. In oncology, perfusion-driven IVIM MRI has already shown its potential for the differential diagnosis of malignant and benign tumors, as well as for detecting prognostic biomarkers and treatment monitoring. Current developments in IVIM data processing, and its use as a method of scanning patients who cannot receive contrast agents, are expected to increase further utilization. This paper reviews the current applications, challenges, and future trends of perfusion-driven IVIM in oncology.

Keywords: *intravoxel incoherent motion, oncology, perfusion, diffusion magnetic resonance imaging*

Introduction

Intravoxel incoherent motion (IVIM) was defined in 1986 by Le Bihan et al.[1] as the "*translational movements* which within a given *voxel* and during the measurement *time* present a *distribution* of *speeds* in *orientation* and/or *amplitude*". Such movements correspond mainly to molecular diffusion, but also to microcirculation of blood in pseudo-randomly oriented capillary vessels and even to tissue vibrations used for MR elastography.[2] The apparent diffusion coefficient (ADC) obtained with diffusion MRI was already shown to include a perfusion related component, especially when very low *b*-values are used.[1] However, it was shown in 1988[3] that perfusion-related effects and diffusion-related effects could be separated within the IVIM composite signal, providing ad hoc acquisition and processing parameters were used. Diffusion MRI is implemented on most clinical MRI systems and today widely used in clinics, and the utility of the ADC in oncology has been very well documented for various organs.[4,5] The potential of perfusion-related IVIM MRI has; however, taken more time to be appreciated, but has enjoyed a significant revival over the past 10 years, as shown in Fig. 1. The reason for perfusion-driven IVIM MRI to lag in time is that IVIM effects are small, requiring very good image quality. With the recent developments in MR hardware and software, which have improved signal-to-noise ratio in IVIM MRI,[6] it is now possible to obtain reliable estimation of perfusion related IVIM parameters. An important feature of IVIM MRI is that it can provide quantitative information on microcirculation without the use of contrast agents, an important advantage in terms of cost, acquisition times and applicability to patients who cannot receive gadolinium-based contrast agents for different reasons. IVIM MRI can provide quantitative maps of the density of small, functional blood vessels (related to flowing blood volume fraction) (Fig. 2), a key component of angiogenesis.[7]

Indeed, the microvasculature of tumors, which often exhibits multiple structural and functional abnormalities, is a major target of oncology treatments. Thus, perfusion imaging has become an important means for the management of cancer, whether for diagnosis, characterization, or staging of malignant tumors associated with active angiogenesis. It is also useful in assessing the response to treatment and detection of recurrence.[8]

Thus far, contrast-enhanced (CE) MRI using gadolinium-based contrast media has been a used as the standard imaging method to assess perfusion in different organs (i.e., brain, spine, abdomen, breast, and heart),[9] because of its better performance compared with other imaging techniques such as CT or ultrasound. CE MRI is highly accurate in evaluating the response to treatment, or assessing for residual disease after neoadjuvant chemotherapy (NAC) of breast cancer.[10–14] The utility of gadoxetic acid as a liver-specific contrast medium is

[1]Department of Diagnostic Imaging and Nuclear Medicine, Kyoto University Graduate School of Medicine, Kyoto, Japan
[2]Department of Clinical Innovative Medicine, Institute for Advancement of Clinical and Translational Science (iACT), Kyoto University Hospital, Kyoto, Japan

*Corresponding author: Department of Diagnostic Imaging and Nuclear Medicine, Kyoto University Graduate School of Medicine, 54, Shogoin-kawaharacho, Sakyo-ku, Kyoto, Kyoto 606-8507, Japan. Phone: +81-75-751-3760, Fax: +81-75-771-9709, E-mail: mamiiima@kuhp.kyoto-u.ac.jp
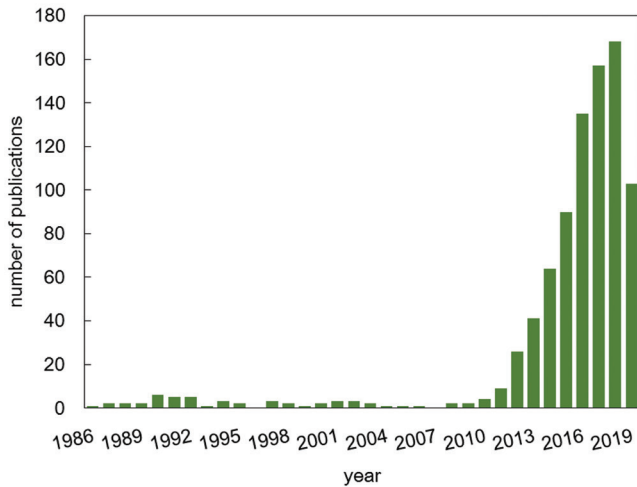
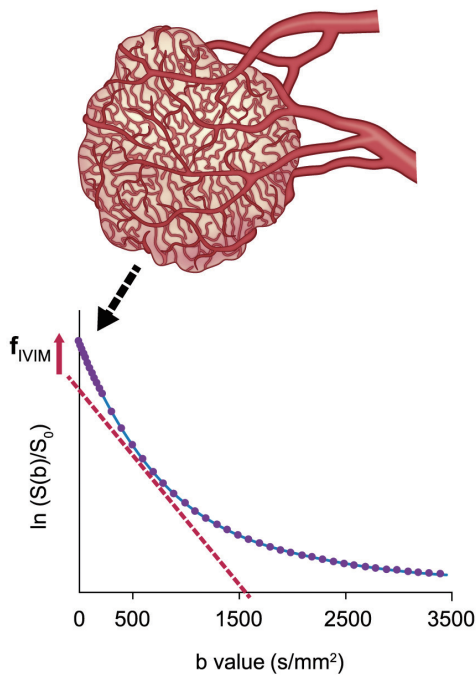**Fig. 1** Number of IVIM publications in 1986–2019.

Fig. 2 Changes in f_{IVIM} with tumor growth. f_{IVIM} increases with the proliferation of neovascularity in some tumors. As the pseudo-diffusion coefficient associated with blood microcirculation is much larger than the true diffusion coefficient in tissues, fast-decaying signal (IVIM effect) appears at low b-values. f_{IVIM}, the flowing blood fraction, increases with the proliferation of neovascularity in some tumors.

recognized for the diagnosis of hepatic lesions.[15] In addition to assessment of vascularity, more advanced CE MRI methods [e.g. dynamic susceptibility contrast (DSC) and dynamic contrast-enhanced (DCE) imaging] provide quantitative and functional information on the tumor microenvironment (e.g. vascular permeability and blood flow).[9] However,

the emergence of contraindications such as nephrogenic systemic fibrosis (NSF) in patients with impaired renal function, as well as reports of gadolinium deposition in the brain and other tissues[16–18] have raised issues, especially when repeated exams are necessary, as in monitoring treatment response and active surveillance for recurrence in oncology.

In this article, after providing a short summary of IVIM MRI principles, the literature showing what perfusion-related IVIM MRI provides in addition to diffusion MRI (and the ADC) for oncologic applications is reviewed.

IVIM Principles

IVIM MRI is sensitive to both molecular diffusion in tissues and to microcirculation (perfusion) based on the assumption that the flow of blood through capillaries mimics a diffusion process, due to the pseudo-random organization of capillaries in tissue. Microcirculation contributes greatly to the diffusion-weighted MRI signal, $S(b)$, together with genuine water molecule diffusion in tissues:

$$\frac{S(b)}{S_0} = f_{IVIM} \ \exp(-b(D_{blood} + D^*)) + (1 - f_{IVIM})Fd \qquad (1)$$

where f_{IVIM} is the flowing blood fraction, D^* is the pseudo-diffusion coefficient associated with blood microcirculation, D_{blood} is the water diffusion coefficient in blood, and Fd, the diffusion-related signal attenuation. Diffusion and perfusion effects can be disentangled from the overall diffusion/IVIM MRI signal because the pseudo-diffusion coefficient associated with blood microcirculation is about ten times larger than the water diffusion coefficient in tissues.

In a simple model assuming diffusion is quasi-Gaussian in tissues (which is only valid at low b-values, in general <600 s/mm² in the body) one has Fd = $\exp(-bD)$ where D is the water diffusion coefficient in tissues. In this case, Eq. (1) has a biexponential shape with a "fast" pseudo-diffusion coefficient ($D^* + D_{blood}$) and a "slow" diffusion coefficient (D). f_{IVIM} is sometimes called "f" or "fp," D^* is sometimes referred to as "Dp," "ADC$_{fast}$," or "ADC$_{high}$," while D is sometimes called "Dt," "ADC$_{slow}$," or "ADC$_{low}$," not to be confused with the standard ADC, whose calculation includes both perfusion-related and genuine diffusion effects.[1]

However, diffusion signal behavior is non-Gaussian in tissues (especially in cancers with high diffusion hindrance or restriction due to cell proliferation), and fitting IVIM signals into Eq. (1) when including moderate or high b-values results in artificially high f-values. In those conditions, a different function, Fd, must be used to take into account non-Gaussian diffusion effects, as the IVIM/diffusion signal attenuation curve is no longer biexponential (for more details, please see "Challenges").

Perfusion MRI Methods in Oncology

Angiogenesis plays an important role in the growth of tumors.[19] Tumor vasculature largely consists of immature and tortuous vessels.[20] The IVIM framework may be able to capture data on microperfusion in many tumors, as has been validated in several studies (please see next sections).

The main MRI perfusion techniques to date are DSC, DCE, and arterial spin labeling (ASL). Both DSC and DCE require administration of gadolinium, while ASL is contrast-free. DSC is widely used for the clinical evaluation of stroke, tumors, and myocardial ischemia, which involves an intravenous bolus of gadolinium chelate and the serial measurement of signal loss by the passage of the bolus on T_2- or T_2^*-weighted images.[21] ASL is mainly used to evaluate blood flow in the brain, heart, kidney, and muscle, and uses the magnetically labeled blood water itself as an endogenous tracer.[22] DCE is widely used for the diagnosis or evaluation of treatment response of tumors, where T_1-weighted images (T_1WI) are acquired dynamically before, during, and after bolus injection of a contrast agent (CA) over approximately 5–10 min to allow visualization of arterial and venous phases, including the portal venous phase in the liver. Gadolinium contrast accumulates within the extracellular space during this time frame, and the signal intensity measurements extract quantitative parameters that reflect tissue perfusion, extravascular extracellular space, and vessel permeability.[23]

Correlation of IVIM parameter f with tumor blood volume obtained with DCE-MRI has been reported in cancers of the head and neck,[24] cervix,[25] and some soft tissue cancers;[26] no correlation has been found in glioma.[27] IVIM reflects all randomly flowing blood in each voxel, while DCE mostly measures CA extravasation, where most of the recorded signals derive from the contrast material accumulating in the interstitial space, so their values will differ.

Validation with Histology

The vasculature considered in IVIM imaging has incoherent flow. Thus, one might expect correlation between IVIM parameters (f or $f \cdot D^*$) and microvasculature histology, such as microvessel area or microvessel density, especially in tumors. There have been several studies published both in humans and animals, as shown in Table 1.[28–38] It is interesting to see that the correlation can be observed both in human tumors and animal xenografts; however, some studies have found no significant correlation. Bakke et al.[32] found no significant correlation between f and microvessel density or vessel size in 12 rectal cancer patients, and Li et al.[38] also found no significant correlation between f and microvessel density in 16 liver tumors in rabbits ($r = 0.281$, $P = 0.291$). Conversely, IVIM parameter maps obtained by clustering approaches with Gaussian mixture models might be useful for the identification of tumor subregions with proliferative

activity (Ki-67 index).[39] Still, the correlation between IVIM parameters (f or $f \cdot D^*$) and microvascular histology is not entirely clear, and further studies are needed to validate the correlation, both in humans and animals.

Several papers have reported the correlation between D and cellularity, however, the correlation between ADC and cellularity has been already extensively investigated in various tumors.

Clinical Applications of IVIM in Oncology

IVIM for characterization and prognostication of tumors

Breast

The diagnostic performance of IVIM parameters for distinguishing between malignant and benign breast tumors has been reported in eight studies.[40,41] Malignant lesions showed significantly lower D in all eight investigations, and seven of the studies demonstrated significantly higher f_{IVIM} values in malignant lesions.[40]

Lower ADC values in estrogen receptor (ER) or progesterone receptor (PgR) positive tumors have already been reported in many papers.[42–61] Kawashima et al.[53] demonstrated significantly lower D and ADC values in luminal B compared with luminal A tumors. Iima et al.[58] reported significantly lower $sADC_{200–1500}$ values in PgR expression. IVIM parameters' correlation with hormone receptors is also worthy of investigation. IVIM histogram analysis revealed a significant correlation of fp and the pseudo-diffusion coefficient (Dp) with hormone receptor expression (ER or PgR),[49] while Kim et al.[50] found that Dp negatively correlated with ER and PgR expression.

Some researchers have also investigated the association of IVIM parameters with pathological biomarkers. Lee et al.[51] found that D_{slow} 50th, 75th, and 90th percentile values were decreased in ER-positive tumors, and f skewness increased in Ki-67 positive tumors. Suo et al.[52] reported that the ER expression significantly correlated with ADC, D and f, and D^* significantly correlated with Ki-67 expression. Significantly lower D^* values in borderline and malignant phyllodes tumors compared with fibroadenomas have been observed, which might reflect a slow blood velocity and have some association with quantity of stroma.[62]

Recent publications have shown the utility of IVIM for monitoring treatment response. Several researchers have reported the utility of D or f for detecting pCR (pathological complete response) after neoadjuvant treatment of breast cancers.[63–65] Che et al.[63] demonstrated pretreatment f-value of pCR group significantly higher than that of non-pCR, and Bedair et al.[64] reported pretreatment diffusion coefficients of pCR group significantly lower than that of non-pCR. Cho et al.[65] showed that histogram metrics of pseudodiffusion Dp significantly differed between response evaluation criteria in solid tumors responders from nonresponders, while ADC or Dt parameters did not.

Table 1 *f*, *D** or *f·D** validation studies with histologic correlation

Humans	Year	Cancer	Subjects (*n*)	Correlation	Correlation coefficient
Bäuerle et al.[28]	2013	Rectal cancer without therapy	12	*f* vs. microvessel area	*r* = 0.60, *P* < 0.05
Bäuerle et al.[28]	2013	Rectal cancer after chemoradiotherapy	9	*f* vs. microvessel area	*r* = −0.44, *P* = 0.29
Klau et al.[29]	2015	Pancreatic adenocarcinoma and PNET	36 and 6	*f* vs. microvessel density	*r* = 0.85, *P* < 0.01
Surov et al.[30]	2017	Rectal cancer	17	*f* vs. microvessel area	*r* = 0.68, *P* = 0.003
Togao et al.[31]	2018	Meningioma	29	*f* vs. microvessel density	*r* = 0.69, *P* < 0.0001
Bakke et al.[32]	2019	Rectal cancer	12	*f·D** vs. microvessel density or vessel size	No significant correlation
Kikuchi et al.[33]	2019	Pediatric intracranial tumors	17	*f* vs. microvessel density	*r* = 0.832, *P* < 0.0001
Animals	Year	Cancer	Subjects (*n*)	Correlation	Correlation coefficient
Iima et al.[34]	2014	Glioma in rats	14	*f* vs. microvessel density	*r* = 0.56, *P* < 0.05
Lee et al.[35]	2014	Colorectal cancer in mice	25	*f*, *D** vs. microvessel density	*f*: *r* = 0.75, *P* < 0.001 *D**: *r* = 0.78, *P* < 0.001
Joo et al.[36]	2014	Liver tumors in rabbits	21	*f*, *f·D** vs. microvessel density	*f*: *r* = 0.52, *P* = 0.02 *fD**: *r* = 0.62, *P* = 0.003
Yang et al.[37]	2017	Hepatocellular carcinoma mouse model not treated	15	*f* vs. microvessel density	*r* = 0.57, *P* = 0.009
Yang et al.[37]	2017	Hepatocellular carcinoma mouse model treated	15	*f* vs. microvessel density	*r* = 0.44, *P* = 0.054
Li et al.[38]	2018	Liver tumors in rabbits	16	*f*, *D** vs. microvessel density	No significant correlation

Brain tumors

Federau et al.[66] showed that *f*-values positively correspond with glioma grade. However, a recent meta-analysis of nine studies in grading gliomas showed higher *D** and lower *D* in high-grade compared to low-grade gliomas, but no correlation of *f* with grade.[67] Puig et al.[68] have reported correlation of *f* and *D** values with cerebral blood flow in glioblastomas, and *f* > 9.86% and *D** > 21.712 × 10^{-3} mm²/s were the thresholds for lower 6-month survival, with both 100% sensitivity and area under the curve (AUC) of 0.893 and 0.857, respectively. Federau et al.[69] have further reported on *f* and ADC values for predicting survival in gliomas, suggesting higher *f* (>0.112), lower ADC (<1033 × 10^{-6} mm²/s) and higher relative cerebral blood volume (>3.01) as the indicators of poorer prognosis, with AUCs predicting a 2-year survival of 0.84 for *f*-value, 0.86 for ADC value, and 0.76 for relative cerebral blood volume.

Head and neck

A recent meta-analysis of the diagnostic performance of combined IVIM parameters in distinguishing among squamous cell carcinomas, lymphomas, malignant salivary gland tumors, Warthin tumors, and pleomorphic adenomas yielded a sensitivity of 85–87% and specificity of 80–100%.[70] One example of IVIM parameters in characterizing perfusion and diffusion properties of head and neck tumors is shown in Fig. 3.[71] Several studies have found significantly smaller *D*- and *f*-values in lymphomas compared with squamous cell carcinomas.[72–75] *D* in malignant salivary gland tumors was also found to be significantly lower than in pleomorphic adenomas, and significantly higher than in Warthin tumors.[72–74] Different numbers and combinations of *b*-values have been used in the head and neck, with a median of 10.5 *b*-values, from 0–800 to 0–1000 s/mm².[70] Significantly higher *f* and lower *D*-values in primary tumors compared with metastatic nodes have been shown in head and neck cancer.[76] Liang et al. demonstrated that *D·D** is the most significant predictor of lymph node metastasis in head and neck squamous carcinoma.[77] Fujima et al.[78] reported that *D*- and *K*-values estimated using a hybrid IVIM and diffusion kurtosis imaging (DKI) model were also found useful in predicting future distant metastasis in head and neck squamous cell carcinoma patients.

Monitoring IVIM MRI parameters during treatment (pattern of low pre-treatment *D* or *f*-values and an increase in *D* during treatment) was found to be useful in predicting response to NAC in head and neck cancers, with 64–94% sensitivity and 72–89% specificity.[70]

Liver

Intravoxel incoherent motion has a potential role in staging liver fibrosis, with a sensitivity of 71–81% and specificity of 77–84%, and *D* has been reported to be significantly lower in malignant compared with benign hepatic tumors.[79] Although
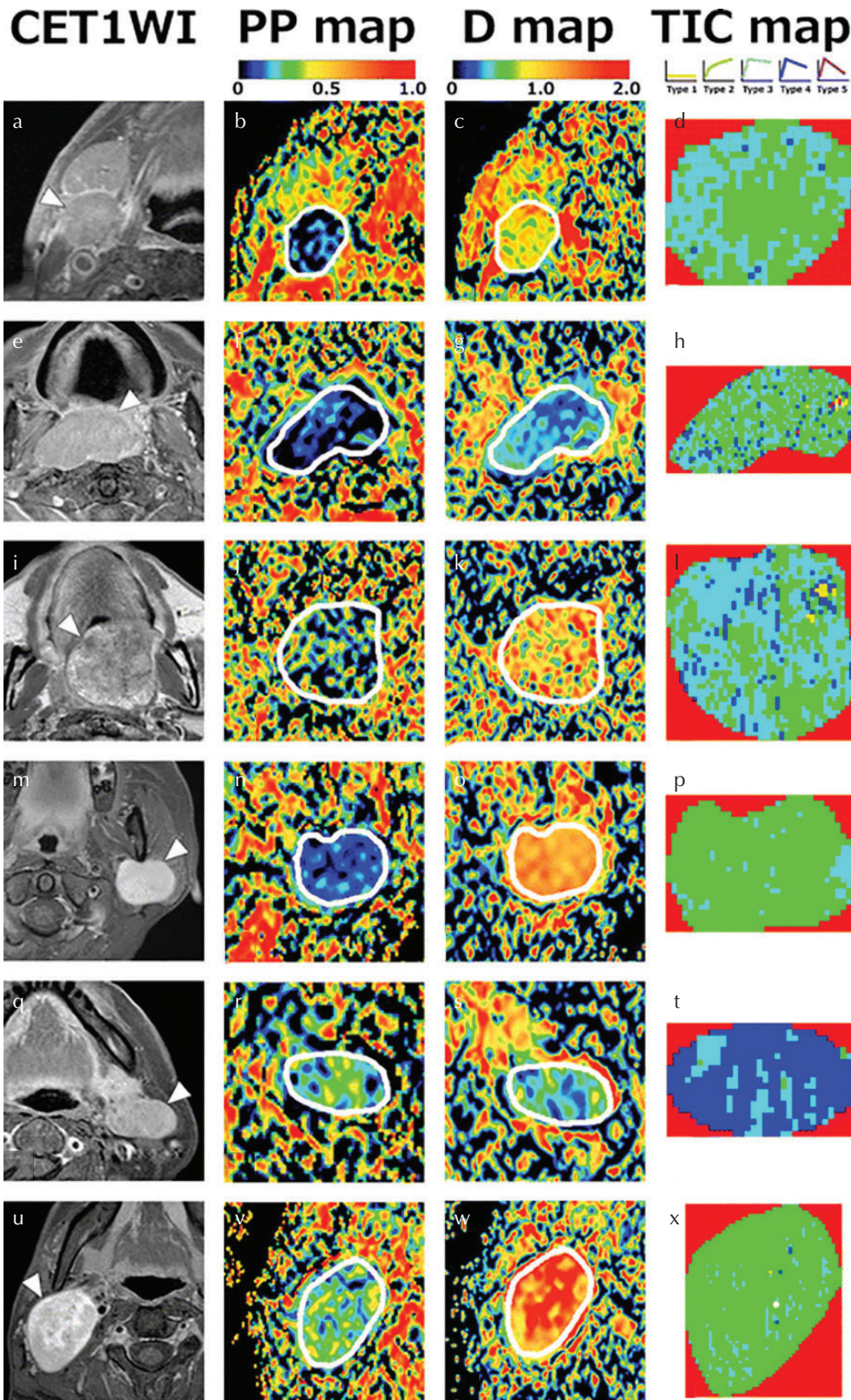
Fig. 3 Representative contrast-enhanced T$_1$-weighted MR images (CE T$_1$WI) with (**a**, **e**, **m**, **q** and **u**) or without (**i**) fat-suppression, and PP, D, and TIC maps of a squamous cell carcinoma (SCC) node (**a**–**d**), lymphoma (**e**–**h**), carcinoma ex pleomorphic adenoma (**i**–**l**), pleomorphic adenoma (**m**–**p**), Warthin tumor (**q**–**t**), and schwannoma (**u**–**x**). (**a**–**d**) A 75-year-old man with an SCC node at level IIA (**a**), PP = 0.057 (**b**), D = 0.830 × 10^{-3} mm^2/s (**c**), TIC profile = Type 2 (**d**). (**e**–**h**) A 79-year-old man with lymphoma in the oropharynx (**e**), PP = 0.04 (**f**), D = 0.435 × 10^{-3} mm^2/s (**g**), TIC profile = Type 3. (**i**–**l**) A 59-year-old man with carcinoma ex pleomorphic adenoma in the palate (**i**), PP = 0.217 (**j**), D = 1.005 × 10^{-3} mm^2/s (**k**), TIC profile = Type 3 (**l**). (**m**–**p**) A 34-year-old woman with pleomorphic adenoma in the left parotid gland (**m**), PP = 0.099 (**n**), D = 1.287 × 10^{-3} mm^2/s (**o**), TIC profile = Type 2 (**p**). (**q**–**t**) A 63-year-old woman with Warthin tumor in the left parotid gland (**q**), PP = 0.227 (**r**), D = 0.485 × 10^{-3} mm^2/s (**s**), TIC profile = Type 4 (**t**). (**u**–**x**) A 24-year-old man with a schwannoma (**u**), PP = 0.294 (**v**), D = 1.550 × 10^{-3} mm^2/s (**w**), TIC profile = Type 2 (**x**). White demarcations on the PP and D maps indicate tumor areas. Adapted from Sumi et al.[71]

there is evidence of an association of D-values with the histological grade of hepatocellular carcinoma (HCC), attempts at finding an association between f and D^* measurements have been inconclusive, and their added value is still controversial.[80] Scholars have investigated the variability of IVIM in grading HCC lesions, depending on the fitting

methods or ROI positioning.[81,82] Ichikawa et al. demonstrated that the choice of fitting methods affects IVIM parameter values, with smaller D-values found in poorly differentiated, compared with well-to-moderately differentiated HCC, using all methods.[81] Wei et al. reported that the effect of different ROI positioning approaches on IVIM and ADC values is significant in HCC lesions, with ADC_{slow} most predictive of grading HCC (a negative correlation with HCC grade) (Fig. 4).[82] Recent investigations have reported the superiority of D or its histogram analysis over ADC in evaluating microvascular invasion in HCC.[83,84]

D^* was reported to be more accurate than ADC in distinguishing responders from non-responders to loco-regional treatment in HCCs;[85] and f-values significantly increased at 2-week follow-up of HCCs responding to sorafenib, while no significant difference was found in ADC or D.[86] However, another group later found no significant differences in f between responders and non-responders.[87]

Pancreas
Among IVIM parameters, several studies reported that f-value was decreased in pancreatic ductal adenocarcinoma (PDAC) compared with normal pancreatic tissue,[88–93] while no significant difference in D-value was found between carcinoma and healthy tissue,[92,93] except some publications.[89,90] f was found to be most useful for the distinction between pancreatic cancer and chronic pancreatitis, with a trend toward higher f-value in chronic pancreatitis than pancreatic cancer.[88,92,94] D- and f-values have also been found useful to distinguish well/moderately differentiated PDAC from poorly differentiated PDAC, with lower D-values and higher f-values in well/moderately differentiated compared with poorly differentiated PDAC.[95] Several groups have reported that pancreatic neuroendocrine tumors show higher f-values than PDAC, which is considered to reflect their hypervascularity.[29,88,89,92]

Prostate
Several studies have examined the utility of prostate IVIM DWI (D or ADC) in distinguishing prostate cancer from benign hyperplasia and normal tissue, revealing conflicting results in the f measurements in malignant and normal tissue.[96,97] The characteristics of IVIM DWI and MR perfusion parameters in prostate tumors and normal tissues have also been investigated.[97,98]

Pang et al.[97] reported that f is significantly increased (7.2% vs. 3.7%) in tumors compared with normal tissues, in
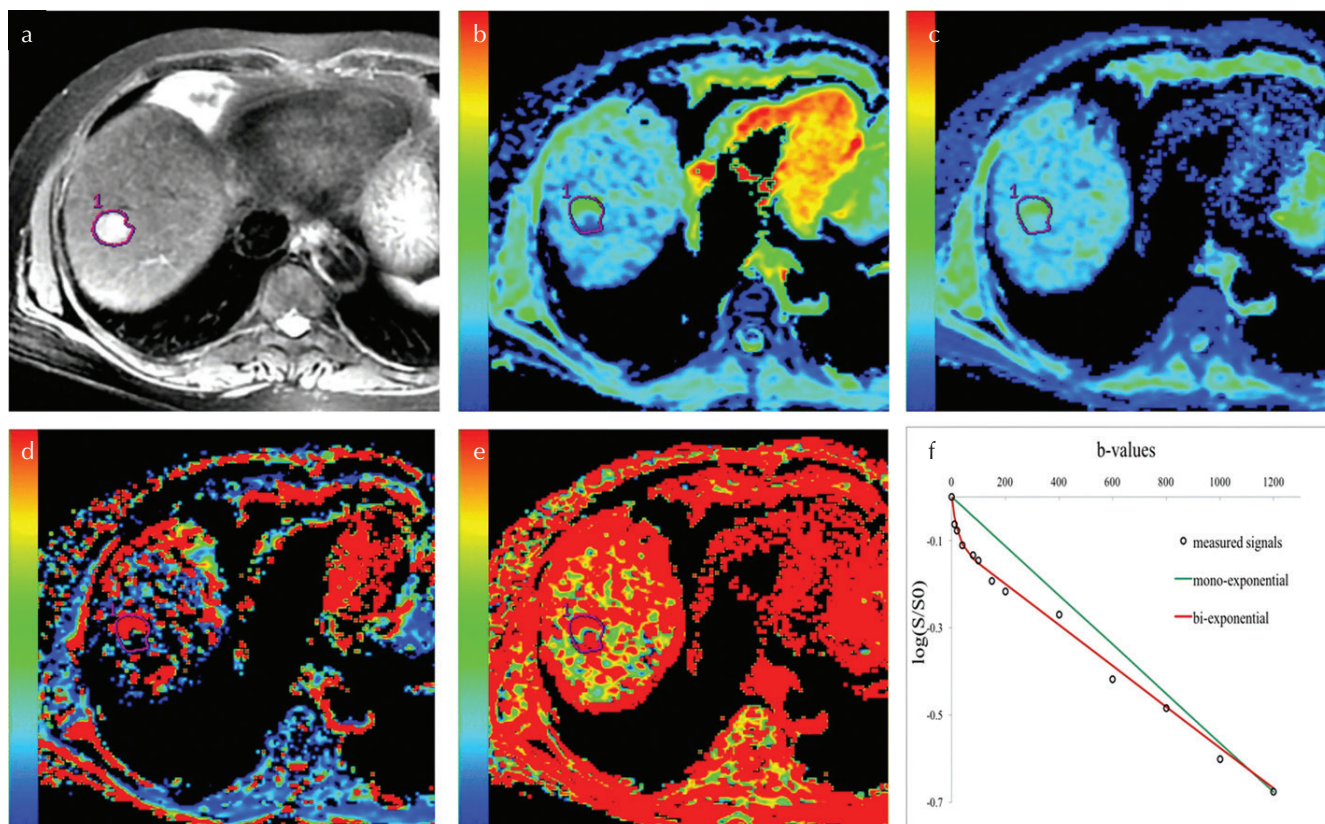

Fig. 4 MR images in a 58-year-old woman with surgically proven HCC of E–S grade 3. (**a**) Portal venous phase image. (**b**) apparent diffusion coefficient (ADC) map. (**c**) ADC_{slow} map. (**d**) ADC_{fast} map. (**e**) and (**f**) map. (**f**) Intravoxel incoherent motion (IVIM) and DWI fitting of the diffusion signal decay. The tumor demonstrates a slightly high signal intensity on T_2-weighted images and blue areas were observed on the ADC and ADC_{slow} map, which indicate a poorly differentiated hepatocellular carcinoma. The IVIM-DWI model achieved significantly better fitting than the DWI. Adapted from Wei et al.[82]

accordance with the volume transfer constant (K_{trans}; 0.39 vs. 0.18/min) and plasma fractional volume (vp; 8.4% vs. 3.4%). Recently, Beyhan et al.[98] also found that the mean values of perfusion parameters obtained from the Tofts model [blood and tissue (K_{trans}), contrast agent back-flux rate constant (K_{ep}), extravascular extracellular fractional volume (V_e), initial area under curve (iAUC) and χ^2] and f significantly increased, and the mean values of Dp and Dt significantly decreased in malignant lesions compared with normal tissue.

Intravoxel incoherent motion histogram metrics might be also useful in the pathological grading of prostate cancers, and it was found that D outperformed conventional ADCs in discriminating low-grade from high-grade prostate cancers.[99]

Female pelvis
The IVIM model has also been intensively investigated in cervical cancer. Poorly differentiated cervical cancer was found to have a lower D than well/moderately differentiated cervical cancer.[100,101] Several studies have reported lower f-values in cervical squamous cell carcinoma (SCC),[101–103] and the results are mixed regarding value for grading of the cervical tumors.[101,103] Interestingly, the f-values at the periphery of cervical cancers were useful in distinguishing tumor grade with higher f in higher-grade tumors,[100] and IVIM histogram metrics distinguished between early and locally advanced cervical cancers.[104] Lee et al.[25] demonstrated that fD^* values positively correlated with DCE-MRI

parameter, $_{est}K^{trans}$ (estimated volume transfer constant between blood plasma, and the extravascular extracellular space, $r = 0.42$, $P = 0.038$). Li et al. recently reported that higher D, f, and V_e values and lower K^{trans} and K_{ep} values were observed in cervical carcinoma with high-expression of HIF-1α. DCE-MRI combined with IVIM DWI had higher sensitivity and accuracy than that of DCE-MRI or IVIM DWI for differentiating the high-expression group and the low-expression group of HIF-1α ($P = 0.03$, 0.02; 0.04, 0.03).[105]

Intravoxel incoherent motion has been assessed in cervical cancer treated with chemoradiotherapy (CRT), and was reported to be an early predictor of treatment response.[106,107] The changes in IVIM parameters (D, D^*, f) and ADC before and during CRT were found to be significantly higher in complete remission (CR) than non-CR groups.[108]

Others
The f-value was found to correlate with ^{18}F-fluorodeoxyglucose positron emission tomography/computed tomography (^{18}F-FDG PET/CT) metabolic parameters in patients with vertebral bone metastases, suggesting its potential for monitoring treatment response.[109] A recent study has shown that histogram analysis of f and D^* may be useful for early response assessment during NAC in osteosarcoma.[110] The utility of IVIM parameters has also been demonstrated in differentiating malignant childhood tumor types (Fig. 5).[111] Other potential
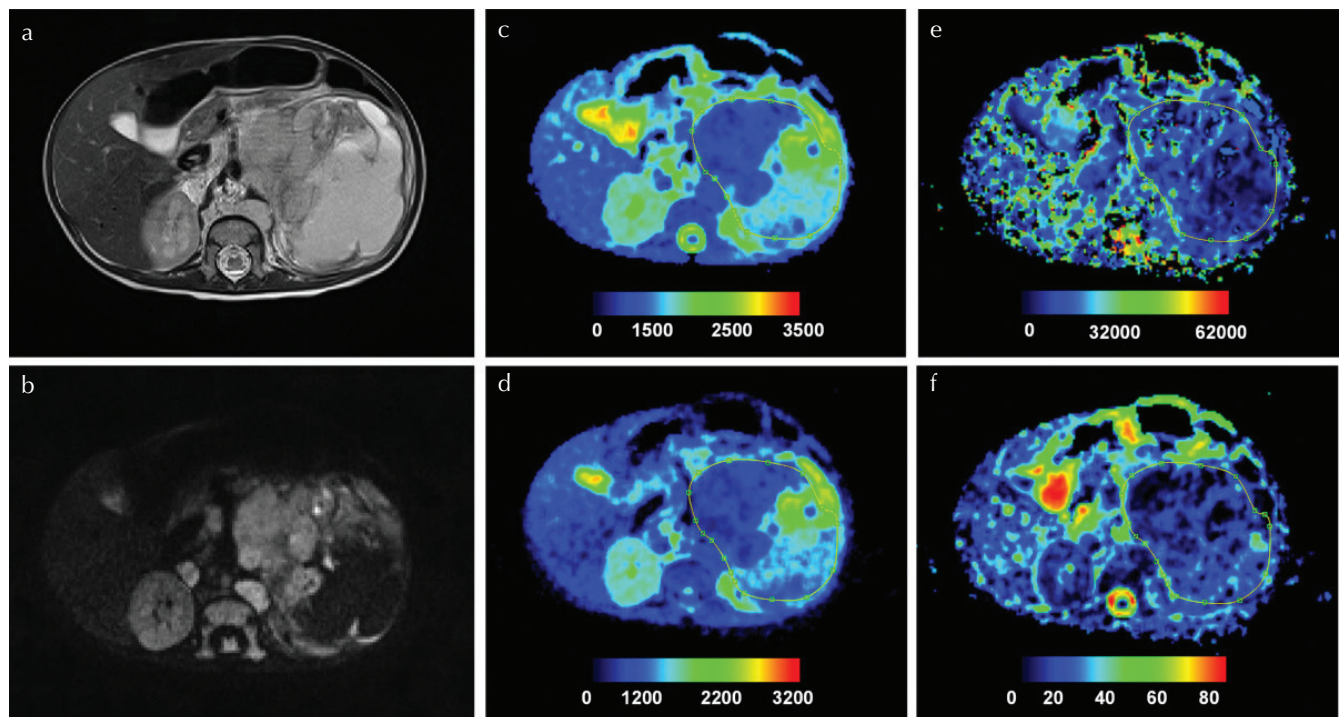

Fig. 5 Histologically verified neuroblastoma (grade IV). (**a**) T_2-weighted and (**b**) $b = 150$ images, and (**c**)–(**f**) parametric maps [apparent diffusion coefficient (ADC), D, D^*, and f, respectively]. Whole tumor ROI is shown drawn on the parametric maps. The calculated median values of ADC, D, D^*, and f for the drawn ROI were 1155×10^{-6} mm^2/s, 703×10^{-6} mm^2/s, $17,762 \times 10^{-6}$ mm^2/s, and 23%, respectively. Adapted from Meeus et al.[111]

clinical applications in oncology include rectal [decrease of ADC, pseudo-diffusion coefficient, and perfusion fraction with poorer tumor differentiation (r = 0.520, P < 0.001; r = 0.447, P = 0.001; r = 0.354, P = 0.010, respectively)],[112] esophageal (higher diagnostic performance of ADC$_{slow}$ than ADC for differentiation of grades of esophageal carcinoma),[113] and lung carcinoma [significantly lower ADC calculated using all b-values, D- and f-values in lung cancer compared with obstructive pulmonary consolidation (P < 0.05)].[114] Despite all these promising results, the clinical application of IVIM parameters for the assessment of treatment response has been limited compared with ADC owing to their only moderate repeatability and reproducibility (please also see "Challenges").[115]

Challenges

There has been a growing number of publications on IVIM in the past 10 years, presumably due to the IVIM "wake up-call" in 2008,[116,117] reporting significant decrease in D^* and ADC values in cirrhotic patients, which has shed some light on clinical applications of IVIM. Additional IVIM models and fitting methods have been explored in various organs and diseases.[118]

One needs to keep in mind that the behavior of DW signals is non-Gaussian (monoexponential for tissue diffusion), especially in highly restricted tissues such as cancers, where departure from a Gaussian distribution appears at b-values as low as 600 s/mm² (the highest b-values reported when the initial biexponential model was introduced were approximately 200 s/mm².) Using the standard biexponential IVIM/diffusion model when including high b-values fails to take this effect into account, and the f fraction becomes artificially high (sometimes >40%) due to the presence of residual tissue diffusion effects in the perfusion-related IVIM part of the signal (this artifact would be the largest in tissues with hindered diffusion, i.e., the most malignant areas). In addition, it is well known that fitting data with the biexponential model through the common least-squares model-fitting approach is sensitive to noise effects and outliers.[34] Thus, development of a more accurate model is crucial, especially in oncology, and many approaches have been proposed (see "Future Trends"). To take care of non-Gaussian and "noise floor" effects visible when higher b-values are used (approximately 1000 s/mm²), more sophisticated models must be used for data analysis. One popular model is the kurtosis model, where non-Gaussianity in diffusion displacement probability distributions of water molecules in tissues can be measured.[6,119,120] Eventually, more effective IVIM and non-Gaussian DWI models might lead to more accurate handling of IVIM parameters.

Intravoxel incoherent motion parameters (especially D^*) have modest repeatability and reproducibility (Table 2),[121–130] perhaps due to their inherent inflexibility in the standard IVIM model and sensitivity to noise,[6] and several approaches have been explored to improve their uncertainty. IVIM values are dependent on the acquisition parameters such as b-values,[118]

Table 2 Repeatability and reproducibility of IVIM parameters in cancers

Authors	Year	Organ	Subjects (n)	Number of b-values	Interval between two scans	Coefficient of variation or (Bland–Altman 95% limits of agreement)		
						f	D^*	D
Andreou et al.[121]	2013	Liver	14	8	1 h	(−75.3, 241.0)	(−89.0, 2120.0)	(−20.8, 25.3)
Kakite et al.[122]	2015	Liver	15	16	5 days	37.3	60.6	19.7
Winfield et al.[123]	2015	Ovary	31	10	3 days	44	165.1	13.2
Jerome et al.[124]	2017	Pediatric solid tumors	15	6	1 day	41	35.1	2.5
Kang et al.[125]	2017	Neck	5	17	10 min	22.1	41.8	8.2
Kang et al.[125]	2017	Neck	5	Four with cardiac gating	10 min	15.3	29.2	5.7
Sun et al.[126]	2017	Rectum	26	8	20–30 min	126.3	197.4	24.5
Lecler et al.[127]	2017	Orbit	22	15	17 min	43	110	14
Pan et al.[128]	2018	Kidney	25	9–16	1–2 days	26.8–50.5	75.5–101.4	11.8–19.1
Jiang et al.[129]	2018	Lung	50	10	0.5–1 h	36.5–38.3	68.6–72.6	11.1–11.3
Iima et al.[130]	2018	Breast	Seven malignant, eight benign	5	Continuous	8.38–16.8	33.4–34.0	–

TE,[131] and fitting methods,[81] and uniform acquisition of IVIM data and development of robust IVIM fitting are warranted. Many efforts are underway to improve the estimation of IVIM parameters. Removal of motion-contaminated and poorly fitted image data has been proposed to improve their reproducibility.[132] The uncertainty of IVIM D and f estimates can be reduced by the use of optimized b-value schemes.[133] Cardiac gating was found useful in improving the reproducibility of IVIM values in the head and neck.[125]

Future Trends

There remain many challenges in IVIM, both in terms of acquisition and processing. There is little standardized software available to estimate IVIM parameters,[40] and DWI data often cannot be processed online in picture archiving and communication systems (PACS). Cooperation with vendors is crucial for the development of software that will work in PACS, as well as to generate robust IVIM parameters, and a one-step approach for the optimization and standardization of acquisition protocols and image processing. Efforts are ongoing for optimizing acquisition schemes such as b-values or number of acquisitions within a clinically feasible scanning time.[133–135] Segmented (or two-step, stepwise, over-segmented, or asymptotic) model fitting has been most commonly used to estimate robust diffusion and perfusion parameters.[118] Several groups have investigated the utility of Bayesian analysis as an alternative to IVIM model-fitting parameter estimation,[136–138] although parameters might be more biased in hypoperfused tissues with this method. Simplified approaches have attempted by several groups to estimate IVIM parameters without fitting;[72,139] for instance, Sumi et al. estimated IVIM parameters using a geometric method, and Teruel et al. introduced relative-enhanced diffusivity (RED), which is based on the relative increase of the ADC values calculated at a low b-value with respect to the ADC values measured at medium b-values. The optimal b-values for RED have also been investigated, and the authors suggest including b-values of 100 in the breast and 50 in the liver for RED.[135]

Integration of artificial intelligence (AI)/machine learning and IVIM in data acquisition and analysis might be an important approach in the future. A recent study showed a machine-learning algorithm combining MRI-derived data including IVIM as a potential predictive biomarker of treatment outcomes in sinonasal SCCs. Deep neural networks have been explored for accurate and robust IVIM or IVIM and non-Gaussian DWI model fitting to DWI data.[140,141]

Other advanced IVIM models are worthy of investigation. Flow-compensated IVIM has been explored, which could be helpful in removing the effect of relatively large vessels on f fraction at the time of acquisition. Diffusion time-dependent IVIM estimates have been demonstrated in the mouse brain; however, significant changes in IVIM values with changing diffusion times have not been identified in xenograft mouse models.[125]

More and more studies have investigated the clinical applications of IVIM in oncology over the past decade. Abundant numbers of approaches and strategies have been extensively explored for optimization of IVIM/diffusion data acquisition and processing. Work remains to improve reproducibility in IVIM parameters and establish the pipeline to analyze IVIM/DWI data online, in cooperation with vendors.

Acknowledgments

Conflicts of Interest

The author declares that there is no conflict of interest.

References

1. Le Bihan D, Breton E, Lallemand D, Grenier P, Cabanis E, Laval-Jeanet M. MR imaging of intravoxel incoherent motions: application to diffusion and perfusion in neurologic disorders. Radiology 1986; 161:401–407.

2. Le Bihan D, Ichikawa S, Motosugi U. Diffusion and intravoxel incoherent motion MR imaging-based virtual elastography: a hypothesis-generating study in the liver. Radiology 2017; 285:609–619.

3. Le Bihan D, Breton E, Lallemand D, Aubin ML, Vignaud J, Laval-Jeanet M. Separation of diffusion and perfusion in intravoxel incoherent motion MR imaging. Radiology 1988; 168:497–505.

4. Padhani AR, Liu G, Koh DM, et al. Diffusion-weighted magnetic resonance imaging as a cancer biomarker: consensus and recommendations. Neoplasia 2009; 11:102–125.

5. Taouli B, Beer AJ, Chenevert T, et al. Diffusion-weighted imaging outside the brain: Consensus statement from an ISMRM-sponsored workshop. J Magn Reson Imaging 2016; 44:521–540.

6. Le Bihan D. What can we see with IVIM MRI? Neuroimage 2019; 187:56–67.

7. Spannuth WA, Sood AK, Coleman RL. Angiogenesis as a strategic target for ovarian cancer therapy. Nat Clin Pract Oncol 2008; 5:194–204.

8. Fass L. Imaging and cancer: a review. Mol Oncol 2008; 2:115–152.

9. Lohrke J, Frenzel T, Endrikat J, et al. 25 Years of contrast-enhanced MRI: developments, current challenges and future perspectives. Adv Ther 2016; 33:1–28.

10. Belli P, Costantini M, Malaspina C, Magistrelli A, LaTorre G, Bonomo L. MRI accuracy in residual disease evaluation

in breast cancer patients treated with neoadjuvant chemotherapy. Clin Radiol 2006; 61:946–953.

11. Segara D, Krop IE, Garber JE, et al. Does MRI predict pathologioc tumor response in women with breast cancer undergoing preoperative chemotherapy? J Surg Oncol 2007; 96:474–480.

12. Rosen EL, Blackwell KL, Baker JA, et al. Accuracy of MRI in the detection of residual breast cancer after neoadjuvant chemotherapy. AJR Am J Roentgenol 2003; 181:1275–1282.

13. Bhattacharyya M, Ryan D, Carpenter R, Vinnicombe S, Gallagher CJ. Using MRI to plan breast-conserving surgery following neoadjuvant chemotherapy for early breast cancer. Br J Cancer 2008; 98:289–293.

14. Prati R, Minami CA, Gornbein JA, Debruhl N, Chung D, Chang HR. Accuracy of clinical evaluation of locally advanced breast cancer in patients receiving neoadjuvant chemotherapy. Cancer 2009; 115:1194–1202.

15. Motosugi U, Ichikawa T, Araki T. Rules, roles, and room for discussion in gadoxetic acid-enhanced magnetic resonance liver imaging: current knowledge and future challenges. Magn Reson Med Sci 2013; 12:161–175.

16. Kanda T, Nakai Y, Oba H, Toyoda K, Kitajima K, Furui S. Gadolinium deposition in the brain. Magn Reson Imaging 2016; 34:1346–1350.

17. Pullicino R, Radon M, Biswas S, Bhojak M, Das K. A review of the current evidence on gadolinium deposition in the brain. Clin Neuroradiol 2018; 28:159–169.

18. Kanda T, Ishii K, Kawaguchi H, Kitajima K, Takenaka D. High signal intensity in the dentate nucleus and globus pallidus on unenhanced T_1-weighted MR images: relationship with increasing cumulative dose of a gadolinium-based contrast material. Radiology 2014; 270:834–841.

19. Pang RW, Poon RT. Clinical implications of angiogenesis in cancers. Vasc Health Risk Manag 2006; 2:97–108.

20. Merlot AM, Kalinowski DS, Richardson DR. Unraveling the mysteries of serum albumin-more than just a serum protein. Front Physiol 2014; 5:299.

21. Kalpathy-Cramer J, Gerstner ER, Emblem KE, Andronesi O, Rosen B. Advanced magnetic resonance imaging of the physical processes in human glioblastoma. Cancer Res 2014; 74:4622–4637.

22. Deibler AR, Pollock JM, Kraft RA, Tan H, Burdette JH, Maldjian JA. Arterial spin-labeling in routine clinical practice, part 1: technique and artifacts. AJNR Am J Neuroradiol 2008; 29:1228–1234.

23. Choyke PL, Dwyer AJ, Knopp MV. Functional tumor imaging with dynamic contrast-enhanced magnetic resonance imaging. J Magn Reson Imaging 2003; 17:509–520.

24. Fujima N, Yoshida D, Sakashita T, et al. Intravoxel incoherent motion diffusion-weighted imaging in head and neck squamous cell carcinoma: assessment of perfusion-related parameters compared to dynamic contrast-enhanced MRI. Magn Reson Imaging 2014; 32:1206–1213.

25. Lee EY, Hui ES, Chan KK, et al. Relationship between intravoxel incoherent motion diffusion-weighted MRI and dynamic contrast-enhanced MRI in tissue perfusion of cervical cancers. J Magn Reson Imaging 2015; 42:454–459.

26. Marzi S, Stefanetti L, Sperati F, Anelli V. Relationship between diffusion parameters derived from intravoxel incoherent motion MRI and perfusion measured by dynamic contrast-enhanced MRI of soft tissue tumors. NMR Biomed 2016; 29:6–14.

27. Bisdas S, Braun C, Skardelly M, et al. Correlative assessment of tumor microcirculation using contrast-enhanced perfusion MRI and intravoxel incoherent motion diffusion-weighted MRI: is there a link between them? NMR Biomed 2014; 27:1184–1191.

28. Bäuerle T, Seyler L, Münter M, et al. Diffusion-weighted imaging in rectal carcinoma patients without and after chemoradiotherapy: a comparative study with histology. Eur J Radiol 2013; 82:444–452.

29. Klau M, Mayer P, Bergmann F, et al. Correlation of histological vessel characteristics and diffusion-weighted imaging intravoxel incoherent motion-derived parameters in pancreatic ductal adenocarcinomas and pancreatic neuroendocrine tumors. Invest Radiol 2015; 50:792–797.

30. Surov A, Meyer HJ, Höhn AK, et al. Correlations between intravoxel incoherent motion (IVIM) parameters and histological findings in rectal cancer: preliminary results. Oncotarget 2017; 8:21974–21983.

31. Togao O, Hiwatashi A, Yamashita K, et al. Measurement of the perfusion fraction in brain tumors with intravoxel incoherent motion MR imaging: validation with histopathological vascular density in meningiomas. Br J Radiol 2018; 91:20170912.

32. Bakke KM, Grøvik E, Meltzer S, et al. Comparison of intravoxel incoherent motion imaging and multiecho dynamic contrast-based MRI in rectal cancer. J Magn Reson Imaging 2019; 50:1114–1124.

33. Kikuchi K, Hiwatashi A, Togao O, et al. Intravoxel incoherent motion MR imaging of pediatric intracranial tumors: correlation with histology and diagnostic utility. AJNR Am J Neuroradiol 2019; 40:878–884.

34. Iima M, Reynaud O, Tsurugizawa T, et al. Characterization of glioma microcirculation and tissue features using intravoxel incoherent motion magnetic resonance imaging in a rat brain model. Invest Radiol 2014; 49:485–490.

35. Lee HJ, Rha SY, Chung YE, et al. Tumor perfusion-related parameter of diffusion-weighted magnetic resonance imaging: correlation with histological microvessel density. Magn Reson Med 2014; 71:1554–1558.

36. Joo I, Lee JM, Han JK, Choi BI. Intravoxel incoherent motion diffusion-weighted MR imaging for monitoring the therapeutic efficacy of the vascular disrupting agent CKD-516 in rabbit VX2 liver tumors. Radiology 2014; 272:417–426.

37. Yang SH, Lin J, Lu F, et al. Evaluation of antiangiogenic and antiproliferative effects of sorafenib by sequential histology and intravoxel incoherent motion diffusion-weighted imaging in an orthotopic hepatocellular carcinoma xenograft model. J Magn Reson Imaging 2017; 45:270–280.

38. Li JL, Ye WT, Liu ZY, et al. Comparison of microvascular perfusion evaluation among IVIM-DWI, CT perfusion imaging and histological microvessel density in rabbit liver VX2 tumors. Magn Reson Imaging 2018; 46:64–69.

39. Jalnefjord O, Montelius M, Arvidsson J, Forssell-Aronsson E, Starck G, Ljungberg M. Data-driven identification of tumor subregions based on intravoxel incoherent motion

reveals association with proliferative activity. Magn Reson Med 2019; 82:1480–1490.

40. Iima M, Honda M, Sigmund EE, Ohno Kishimoto A, Kataoka M, Togashi K. Diffusion MRI of the breast: current status and future directions. J Magn Reson Imaging 2020; 52:70–90.

41. Partridge SC, Nissan N, Rahbar H, Kitsch AE, Sigmund EE. Diffusion-weighted breast MRI: clinical applications and emerging techniques. J Magn Reson Imaging 2017; 45:337–355.

42. Kim SH, Cha ES, Kim HS, et al. Diffusion-weighted imaging of breast cancer: correlation of the apparent diffusion coefficient value with prognostic factors. J Magn Reson Imaging 2009; 30:615–620.

43. Jeh SK, Kim SH, Kim HS, et al. Correlation of the apparent diffusion coefficient value and dynamic magnetic resonance imaging findings with prognostic factors in invasive ductal carcinoma. J Magn Reson Imaging 2011; 33:102–109.

44. Choi SY, Chang YW, Park HJ, Kim HJ, Hong SS, Seo DY. Correlation of the apparent diffusion coefficiency values on diffusion-weighted imaging with prognostic factors for breast cancer. Br J Radiol 2012; 85:e474–e479.

45. Martincich L, Deantoni V, Bertotto I, et al. Correlations between diffusion-weighted imaging and breast cancer biomarkers. Eur Radiol 2012; 22:1519–1528.

46. Kamitani T, Matsuo Y, Yabuuchi H, et al. Correlations between apparent diffusion coefficient values and prognostic factors of breast cancer. Magn Reson Med Sci 2013; 12:193–199.

47. Kim EJ, Kim SH, Park GE, et al. Histogram analysis of apparent diffusion coefficient at 3.0t: correlation with prognostic factors and subtypes of invasive ductal carcinoma. J Magn Reson Imaging 2015; 42:1666–1678.

48. Park SH, Choi HY, Hahn SY. Correlations between apparent diffusion coefficient values of invasive ductal carcinoma and pathologic factors on diffusion-weighted MRI at 3.0 Tesla. J Magn Reson Imaging 2015; 41:175–182.

49. Cho GY, Moy L, Kim SG, et al. Evaluation of breast cancer using intravoxel incoherent motion (IVIM) histogram analysis: comparison with malignant status, histological subtype, and molecular prognostic factors. Eur Radiol 2016; 26:2547–2558.

50. Kim Y, Ko K, Kim D, et al. Intravoxel incoherent motion diffusion-weighted MR imaging of breast cancer: association with histopathological features and subtypes. Br J Radiol 2016; 89:20160140.

51. Lee YJ, Kim SH, Kang BJ, et al. Intravoxel incoherent motion (IVIM)-derived parameters in diffusion-weighted MRI: associations with prognostic factors in invasive ductal carcinoma. J Magn Reson Imaging 2017; 45:1394–1406.

52. Suo S, Cheng F, Cao M, et al. Multiparametric diffusion-weighted imaging in breast lesions: association with pathologic diagnosis and prognostic factors. J Magn Reson Imaging 2017; 46:740–750.

53. Kawashima H, Miyati T, Ohno N, et al. Differentiation between luminal-A and luminal-B breast cancer using intravoxel incoherent motion and dynamic contrast-enhanced magnetic resonance imaging. Acad Radiol 2017; 24:1575–1581.

54. Amornsiripanitch N, Nguyen VT, Rahbar H, et al. Diffusion-weighted MRI characteristics associated with prognostic pathological factors and recurrence risk in invasive ER+/HER2- breast cancers. J Magn Reson Imaging 2018; 48:226–236.

55. Shen L, Zhou G, Tong T, et al. ADC at 3.0 T as a noninvasive biomarker for preoperative prediction of Ki67 expression in invasive ductal carcinoma of breast. Clin Imaging 2018; 52:16–22.

56. Liu F, Wang M, Li H. Role of perfusion parameters on DCE-MRI and ADC values on DWMRI for invasive ductal carcinoma at 3.0 Tesla. World J Surg Oncol 2018; 16:239.

57. Fan M, He T, Zhang P, et al. Diffusion-weighted imaging features of breast tumours and the surrounding stroma reflect intrinsic heterogeneous characteristics of molecular subtypes in breast cancer. NMR Biomed 2018; 31. doi: 10.1002/nbm.3869.

58. Iima M, Kataoka M, Kanao S, et al. Intravoxel incoherent motion and quantitative non-Gaussian diffusion MR imaging: evaluation of the diagnostic and prognostic value of several markers of malignant and benign breast lesions. Radiology 2018; 287:432–441.

59. Vidić I, Egnell L, Jerome NP, et al. Support vector machine for breast cancer classification using diffusion-weighted MRI histogram features: preliminary study. J Magn Reson Imaging 2018; 47:1205–1216.

60. Horvat JV, Bernard-Davila B, Helbich TH, et al. Diffusion-weighted imaging (DWI) with apparent diffusion coefficient (ADC) mapping as a quantitative imaging biomarker for prediction of immunohistochemical receptor status, proliferation rate, and molecular subtypes of breast cancer. J Magn Reson Imaging 2019; 50:836–846.

61. Suo S, Zhang D, Cheng F, et al. Added value of mean and entropy of apparent diffusion coefficient values for evaluating histologic phenotypes of invasive ductal breast cancer with MR imaging. Eur Radiol 2019; 29:1425–1434.

62. Kawashima H, Miyati T, Ohno N, et al. Differentiation between phyllodes tumours and fibroadenomas using intravoxel incoherent motion magnetic resonance imaging: comparison with conventional diffusion-weighted imaging. Br J Radiol 2018; 91:20170687.

63. Che S, Zhao X, Ou Y, et al. Role of the intravoxel incoherent motion diffusion weighted imaging in the pre-treatment prediction and early response monitoring to neoadjuvant chemotherapy in locally advanced breast cancer. Medicine (Baltimore) 2016; 95:e2420.

64. Bedair R, Priest AN, Patterson AJ, et al. Assessment of early treatment response to neoadjuvant chemotherapy in breast cancer using non-mono-exponential diffusion models: a feasibility study comparing the baseline and mid-treatment MRI examinations. Eur Radiol 2017; 27:2726–2736.

65. Cho GY, Gennaro L, Sutton EJ, et al. Intravoxel incoherent motion (IVIM) histogram biomarkers for prediction of neoadjuvant treatment response in breast cancer patients. Eur J Radiol Open 2017; 4:101–107.

66. Federau C, Meuli R, O'Brien K, Maeder P, Hagmann P. Perfusion measurement in brain gliomas with intravoxel incoherent motion MRI. AJNR Am J Neuroradiol 2014; 35:256–262.

67. Li WF, Niu C, Shakir TM, Chen T, Zhang M, Wang Z. An evidence-based approach to assess the accuracy of intravoxel incoherent motion imaging for the grading of brain tumors. Medicine (Baltimore) 2018; 97:e13217.

68. Puig J, Sánchez-González J, Blasco G, et al. Intravoxel incoherent motion metrics as potential biomarkers for survival in glioblastoma. PLoS One 2016; 11:e0158887.

69. Federau C, Cerny M, Roux M, et al. IVIM perfusion fraction is prognostic for survival in brain glioma. Clin Neuroradiol 2017; 27:485–492.

70. Noij DP, Martens RM, Marcus JT, et al. Intravoxel incoherent motion magnetic resonance imaging in head and neck cancer: a systematic review of the diagnostic and prognostic value. Oral Oncol 2017; 68:81–91.

71. Sumi M, Nakamura T. Head and neck tumours: combined MRI assessment based on IVIM and TIC analyses for the differentiation of tumors of different histological types. Eur Radiol 2014; 24:223–231.

72. Sasaki M, Sumi M, Eida S, Katayama I, Hotokezaka Y, Nakamura T. Simple and reliable determination of intravoxel incoherent motion parameters for the differential diagnosis of head and neck tumors. PLoS One 2014; 9:e112866.

73. Sumi M, Nakamura T. Head and neck tumors: assessment of perfusion-related parameters and diffusion coefficients based on the intravoxel incoherent motion model. AJNR Am J Neuroradiol 2013; 34:410–416.

74. Sumi M, Van Cauteren M, Sumi T, Obara M, Ichikawa Y, Nakamura T. Salivary gland tumors: use of intravoxel incoherent motion MR imaging for assessment of diffusion and perfusion for the differentiation of benign from malignant tumors. Radiology 2012; 263:770–777.

75. Yu XP, Hou J, Li FP, et al. Intravoxel incoherent motion diffusion weighted magnetic resonance imaging for differentiation between nasopharyngeal carcinoma and lymphoma at the primary site. J Comput Assist Tomogr 2016; 40:413–418.

76. Lu Y, Jansen JF, Stambuk HE, et al. Comparing primary tumors and metastatic nodes in head and neck cancer using intravoxel incoherent motion imaging: a preliminary experience. J Comput Assist Tomogr 2013; 37:346–352.

77. Liang L, Luo X, Lian Z, et al. Lymph node metastasis in head and neck squamous carcinoma: efficacy of intravoxel incoherent motion magnetic resonance imaging for the differential diagnosis. Eur J Radiol 2017; 90:159–165.

78. Fujima N, Sakashita T, Homma A, Yoshida D, Kudo K, Shirato H. Utility of a hybrid IVIM-DKI model to predict the development of distant metastasis in head and neck squamous cell carcinoma patients. Magn Reson Med Sci 2018; 17:21–27.

79. Jiang H, Chen J, Gao R, Huang Z, Wu M, Song B. Liver fibrosis staging with diffusion-weighted imaging: a systematic review and meta-analysis. Abdom Radiol (NY) 2017; 42:490–501.

80. Granata V, Fusco R, Filice S, et al. The current role and future prospectives of functional parameters by diffusion weighted imaging in the assessment of histologic grade of HCC. Infect Agent Cancer 2018; 13:23.

81. Ichikawa S, Motosugi U, Hernando D, et al. Histological grading of hepatocellular carcinomas with intravoxel incoherent motion diffusion-weighted imaging: inconsistent results depending on the fitting method. Magn Reson Med Sci 2018; 17:168–173.

82. Wei Y, Gao F, Wang M, et al. Intravoxel incoherent motion diffusion-weighted imaging for assessment of histologic grade of hepatocellular carcinoma: comparison of three methods for positioning region of interest. Eur Radiol 2019; 29:535–544.

83. Li H, Zhang J, Zheng Z, et al. Preoperative histogram analysis of intravoxel incoherent motion (IVIM) for predicting microvascular invasion in patients with single hepatocellular carcinoma. Eur J Radiol 2018; 105:65–71.

84. Wei Y, Huang Z, Tang H, et al. IVIM improves preoperative assessment of microvascular invasion in HCC. Eur Radiol 2019; 29:5403–5414.

85. Mürtz P, Penner AH, Pfeiffer AK, et al. Intravoxel incoherent motion model–based analysis of diffusion-weighted magnetic resonance imaging with 3 b-values for response assessment in locoregional therapy of hepatocellular carcinoma. Onco Targets Ther 2016; 9:6425–6433.

86. Lewin M, Fartoux L, Vignaud A, Arrivé L, Menu Y, Rosmorduc O. The diffusion-weighted imaging perfusion fraction f is a potential marker of sorafenib treatment in advanced hepatocellular carcinoma: a pilot study. Eur Radiol 2011; 21:281–290.

87. Shirota N, Saito K, Sugimoto K, Takara K, Moriyasu F, Tokuuye K. Intravoxel incoherent motion MRI as a biomarker of sorafenib treatment for advanced hepatocellular carcinoma: a pilot study. Cancer Imaging 2016; 16:1.

88. Concia M, Sprinkart AM, Penner AH, et al. Diffusion-weighted magnetic resonance imaging of the pancreas: diagnostic benefit from an intravoxel incoherent motion model-based 3 b-value analysis. Invest Radiol 2014; 49:93–100.

89. Lee SS, Byun JH, Park BJ, et al. Quantitative analysis of diffusion-weighted magnetic resonance imaging of the pancreas: usefulness in characterizing solid pancreatic masses. J Magn Reson Imaging 2008; 28:928–936.

90. Lemke A, Laun FB, Klauss M, et al. Differentiation of pancreas carcinoma from healthy pancreatic tissue using multiple b-values: comparison of apparent diffusion coefficient and intravoxel incoherent motion derived parameters. Invest Radiol 2009; 44:769–775.

91. Re TJ, Lemke A, Klauss M, et al. Enhancing pancreatic adenocarcinoma delineation in diffusion derived intravoxel incoherent motion f-maps through automatic vessel and duct segmentation. Magn Reson Med 2011; 66:1327–1332.

92. Kang KM, Lee JM, Yoon JH, Kiefer B, Han JK, Choi BI. Intravoxel incoherent motion diffusion-weighted MR imaging for characterization of focal pancreatic lesions. Radiology 2014; 270:444–453.

93. Kim B, Lee SS, Sung YS, et al. Intravoxel incoherent motion diffusion-weighted imaging of the pancreas: characterization of benign and malignant pancreatic pathologies. J Magn Reson Imaging 2017; 45:260–269.

94. Klauss M, Lemke A, Grünberg K, et al. Intravoxel incoherent motion MRI for the differentiation between mass forming chronic pancreatitis and pancreatic carcinoma. Invest Radiol 2011; 46:57–63.

95. Ma W, Zhang G, Ren J, et al. Quantitative parameters of intravoxel incoherent motion diffusion weighted imaging (IVIM-DWI): potential application in predicting pathological grades of pancreatic ductal adenocarcinoma. Quant Imaging Med Surg 2018; 8:301–310.

96. Shinmoto H, Tamura C, Soga S, et al. An intravoxel incoherent motion diffusion-weighted imaging study of prostate cancer. AJR Am J Roentgenol 2012; 199:W496–W500.

97. Pang Y, Turkbey B, Bernardo M, et al. Intravoxel incoherent motion MR imaging for prostate cancer: an evaluation of perfusion fraction and diffusion coefficient derived from different b-value combinations. Magn Reson Med 2013; 69:553–562.

98. Beyhan M, Sade R, Koc E, Adanur S, Kantarci M. The evaluation of prostate lesions with IVIM DWI and MR perfusion parameters at 3T MRI. Radiol Med 2019; 124:87–93.

99. Zhang YD, Wang Q, Wu CJ, et al. The histogram analysis of diffusion-weighted intravoxel incoherent motion (IVIM) imaging for differentiating the gleason grade of prostate cancer. Eur Radiol 2015; 25:994–1004.

100. Zhou Y, Liu J, Liu C, et al. Intravoxel incoherent motion diffusion weighted MRI of cervical cancer - correlated with tumor differentiation and perfusion. Magn Reson Imaging 2016; 34:1050–1056.

101. Lin M, Yu X, Chen Y, et al. Contribution of mono-exponential, bi-exponential and stretched exponential model-based diffusion-weighted MR imaging in the diagnosis and differentiation of uterine cervical carcinoma. Eur Radiol 2017; 27:2400–2410.

102. Li X, Wang P, Li D, et al. Intravoxel incoherent motion MR imaging of early cervical carcinoma: correlation between imaging parameters and tumor-stroma ratio. Eur Radiol 2018; 28:1875–1883.

103. Winfield JM, Orton MR, Collins DJ, et al. Separation of type and grade in cervical tumours using non-mono-exponential models of diffusion-weighted MRI. Eur Radiol 2017; 27:627–636.

104. Thapa D, Wang P, Wu G, Wang X, Sun Q. A histogram analysis of diffusion and perfusion features of cervical cancer based on intravoxel incoherent motion magnetic resonance imaging. Magn Reson Imaging 2019; 55:103–111.

105. Li X, Wu S, Li D, et al. Intravoxel incoherent motion combined with dynamic contrast-enhanced perfusion MRI of Early cervical carcinoma: correlations between multimodal parameters and HIF-1α expression. J Magn Reson Imaging 2019; 50:918–929.

106. Zhu L, Wang H, Zhu L, et al. Predictive and prognostic value of intravoxel incoherent motion (IVIM) MR imaging in patients with advanced cervical cancers undergoing concurrent chemo-radiotherapy. Sci Rep 2017; 7:11635.

107. Zhu L, Zhu L, Wang H, et al. Predicting and early monitoring treatment efficiency of cervical cancer under concurrent chemoradiotherapy by intravoxel incoherent motion magnetic resonance imaging. J Comput Assist Tomogr 2017; 41:422–429.

108. Kato H, Esaki K, Yamaguchi T, et al. Predicting early response to chemoradiotherapy for uterine cervical cancer using intravoxel incoherent motion MR imaging. Magn Reson Med Sci 2019; 18:293–298.

109. Park S, Yoon JK, Chung NS, et al. Correlations between intravoxel incoherent motion diffusion-weighted MR imaging parameters and 18F-FDG PET/CT metabolic parameters in patients with vertebral bone metastases: initial experience. Br J Radiol 2018; 91:20170889.

110. Baidya Kayal E, Kandasamy D, Khare K, Bakhshi S, Sharma R, Mehndiratta A. Intravoxel incoherent motion (IVIM) for response assessment in patients with osteosarcoma undergoing neoadjuvant chemotherapy. Eur J Radiol 2019; 119:108635.

111. Meeus EM, Zarinabad N, Manias KA, et al. Diffusion-weighted MRI and intravoxel incoherent motion model for diagnosis of pediatric solid abdominal tumors. J Magn Reson Imaging 2018; 47:1475–1486.

112. Sun H, Xu Y, Song A, Shi K, Wang W. Intravoxel incoherent motion MRI of rectal cancer: correlation of diffusion and perfusion characteristics with prognostic tumor markers. AJR Am J Roentgenol 2018; 210:W139–W147.

113. Zhu S, Wei Y, Gao F, et al. Esophageal carcinoma: intravoxel incoherent motion diffusion-weighted MRI parameters and histopathological correlations. J Magn Reson Imaging 2019; 49:253–261.

114. Wang LL, Lin J, Liu K, et al. Intravoxel incoherent motion diffusion-weighted MR imaging in differentiation of lung cancer from obstructive lung consolidation: comparison and correlation with pharmacokinetic analysis from dynamic contrast-enhanced MR imaging. Eur Radiol 2014; 24:1914–1922.

115. Koh DM. Science to practice: can intravoxel incoherent motion diffusion-weighted MR imaging be used to assess tumor response to antivascular drugs? Radiology 2014; 272:307–308.

116. Le Bihan D. Intravoxel incoherent motion perfusion MR imaging: a wake-up call. Radiology 2008; 249:748–752.

117. Luciani A, Vignaud A, Cavet M, et al. Liver cirrhosis: intravoxel incoherent motion MR imaging—pilot study. Radiology 2008; 249:891–899.

118. Le Bihan D, Iima M, Federau C, Sigmund EE. Intravoxel incoherent motion (IVIM) MRI: principles and applications. Singapore, Jenny Stanford Publishing, 2018; 1–533.

119. Iima M, Yano K, Kataoka M, et al. Quantitative non-Gaussian diffusion and intravoxel incoherent motion magnetic resonance imaging: differentiation of malignant and benign breast lesions. Invest Radiol 2015; 50:205–211.

120. Jensen JH, Helpern JA, Ramani A, Lu H, Kaczynski K. Diffusional kurtosis imaging: the quantification of non-gaussian water diffusion by means of magnetic resonance imaging. Magn Reson Med 2005; 53:1432–1440.

121. Andreou A, Koh DM, Collins DJ, et al. Measurement reproducibility of perfusion fraction and pseudodiffusion coefficient derived by intravoxel incoherent motion diffusion-weighted MR imaging in normal liver and metastases. Eur Radiol 2013; 23:428–434.

122. Kakite S, Dyvorne H, Besa C, et al. Hepatocellular carcinoma: short-term reproducibility of apparent diffusion coefficient and intravoxel incoherent motion parameters at 3.0T. J Magn Reson Imaging 2015; 41:149–156.

123. Winfield JM, deSouza NM, Priest AN, et al. Modelling DW-MRI data from primary and metastatic ovarian tumours. Eur Radiol 2015; 25:2033–2040.

124. Jerome NP, Miyazaki K, Collins DJ, et al. Repeatability of derived parameters from histograms following non-Gaussian diffusion modelling of diffusion-weighted

imaging in a paediatric oncological cohort. Eur Radiol 2017; 27:345–353.

125. Kang KM, Choi SH, Kim DE, et al. Application of cardiac gating to improve the reproducibility of intravoxel incoherent motion measurements in the head and neck. Magn Reson Med Sci 2017; 16:190–202.

126. Sun H, Xu Y, Xu Q, Shi K, Wang W. Rectal cancer: short-term reproducibility of intravoxel incoherent motion parameters in 3.0T magnetic resonance imaging. Medicine (Baltimore) 2017; 96:e6866.

127. Lecler A, Savatovsky J, Balvay D, et al. Repeatability of apparent diffusion coefficient and intravoxel incoherent motion parameters at 3.0 Tesla in orbital lesions. Eur Radiol 2017; 27:5094–5103.

128. Pan J, Zhang H, Man F, et al. Measurement and scan reproducibility of parameters of intravoxel incoherent motion in renal tumor and normal renal parenchyma: a preliminary research at 3.0 T MR. Abdom Radiol (NY) 2018; 43:1739–1748.

129. Jiang J, Yin J, Cui L, et al. Lung cancer: short-term reproducibility of intravoxel incoherent motion parameters and apparent diffusion coefficient at 3T. J Magn Reson Imaging 2018; 47:1003–1012.

130. Iima M, Kataoka M, Kanao S, et al. Variability of non-Gaussian diffusion MRI and intravoxel incoherent motion (IVIM) measurements in the breast. PLoS One 2018; 13:e0193444.

131. Feng Z, Min X, Wang L, et al. Effects of echo time on IVIM quantification of the normal prostate. Sci Rep 2018; 8:2572.

132. Chevallier O, Zhou N, He J, Loffroy R, Wáng YXJ. Removal of evidential motion-contaminated and poorly fitted image data improves IVIM diffusion MRI parameter scan-rescan reproducibility. Acta Radiol 2018; 59:1157–1167.

133. Jalnefjord O, Montelius M, Starck G, Ljungberg M. Optimization of b-value schemes for estimation of the diffusion coefficient and the perfusion fraction with segmented intravoxel incoherent motion model fitting. Magn Reson Med 2019; 82:1541–1552.

134. Meeus EM, Novak J, Dehghani H, Peet AC. Rapid measurement of intravoxel incoherent motion (IVIM) derived perfusion fraction for clinical magnetic resonance imaging. MAGMA 2018; 31:269–283.

135. While PT, Teruel JR, Vidić I, Bathen TF, Goa PE. Relative enhanced diffusivity: noise sensitivity, protocol optimization, and the relation to intravoxel incoherent motion. MAGMA 2018; 31:425–438.

136. Gustafsson O, Montelius M, Starck G, Ljungberg M. Impact of prior distributions and central tendency measures on Bayesian intravoxel incoherent motion model fitting. Magn Reson Med 2018; 79:1674–1683.

137. Orton MR, Collins DJ, Koh DM, Leach MO. Improved intravoxel incoherent motion analysis of diffusion weighted imaging by data driven Bayesian modeling. Magn Reson Med 2014; 71:411–420.

138. While PT. A comparative simulation study of bayesian fitting approaches to intravoxel incoherent motion modeling in diffusion-weighted MRI. Magn Reson Med 2017; 78:2373–2387.

139. Teruel JR, Goa PE, Sjøbakk TE, Østlie A, Fjøsne HE, Bathen TF. A simplified approach to measure the effect of the microvasculature in diffusion-weighted MR imaging applied to breast tumors: preliminary results. Radiology 2016; 281:373–381.

140. Barbieri S, Gurney-Champion OJ, Klaassen R, Thoeny HC. Deep learning how to fit an intravoxel incoherent motion model to diffusion-weighted MRI. Magn Reson Med 2020; 83:312–321.

141. Bertleff M, Domsch S, Weingärtner S, et al. Diffusion parameter mapping with the combined intravoxel incoherent motion and kurtosis model using artificial neural networks at 3 T. NMR Biomed 2017; 30:e3833.